Precision Agriculture

APPLICATION OF A LOW-COST CAMERA ON A UAV TO ESTIMATE MAIZE NITROGEN-RELATED VARIABLES

--Manuscript Draft--

Manuscript Number:	
Full Title:	APPLICATION OF A LOW-COST CAMERA ON A UAV TO ESTIMATE MAIZE NITROGEN-RELATED VARIABLES
Article Type:	Manuscript
Keywords:	CIR camera; UAV; colorgrams; vegetation indices; maize
Corresponding Author:	Martina Corti, Ph.D. Universita degli Studi di Milano Facolta di Scienze Agrarie e Alimentari ITALY
Corresponding Author's Institution:	Universita degli Studi di Milano Facolta di Scienze Agrarie e Alimentari
First Author:	Martina Corti, Ph.D.
Order of Authors:	Martina Corti, Ph.D.
	Daniele Cavalli
	Giovanni Cabassi
	Antonio Vigoni
	Luigi Degano
	Pietro Marino Gallina
Funding Information:	MIPAAF (D.M n°27335/7303/10) — Not applicable
Suggested Reviewers:	Toshihiro Sakamoto Ecosystem Informatics Division, National Institute for Agro-Environmental Sciences sakamt@affrc.go.jp Expert of digital camera applied to agriculture
	S.L. Osborne USDA-ARS, Northern Grain Insects Research Laboratory sosborne@ngirl.ars.usda.gov Expert in airborne remote sensing of crops
	H. Noh Dept. of Biosystems Engineering, Chungbuk National University nhkisg@cbnu.ac.kr Expert in the use of digital camera for agricultural application
	CC Lelong CIRAD, UMR TETIS camille.lelong@cirad.fr Expert in the use of UAV-mounted digital camera in agriculture
	V Lebourgeois CIRAD UPR SCA valentine.lebourgeois@cirad.fr Expert in UAV-based crop monitoring

APPLICATION OF A LOW-COST CAMERA ON A UAV TO ESTIMATE MAIZE NITROGEN-RELATED VARIABLES

Martina Corti[1], Daniele Cavalli [1], Giovanni Cabassi[2], Antonio Vigoni[3], Luigi Degano[2], Pietro Marino Gallina[1]

[1]Department of Agricultural and Environmental Sciences - Production, Landscape, Agroenergy, Università degli Studi di Milano; via Celoria 2, 20133 Milano (Italy)

[2]Consiglio per la ricerca in agricoltura e l'analisi dell'economia agraria, CREA-ZA; via Antonio Lombardo 11, 26900 Lodi (Italy)

[3] Sport Turf Consulting-Servizi per l'agricoltura con aeromobili a pilotaggio remoto; Via Cesare Battisti, 19, 20027 Rescaldina (MI)

Corresponding Author: Martina Corti, martina.corti@unimi.it

Authors email address: Daniele Cavalli, daniele.cavalli@unimi.it; Giovanni Cabassi, giovanni.cabassi@crea.gov.it; Antonio Vigoni, stc@turfgrass.it; Luigi Degano, luigi.degano@crea.gov.it; Pietro Marino Gallina, pietro.marino@unimi.it.

ABSTRACT

The development of small unmanned aerial vehicles (UAVs) and advancements in sensors technology made consumer digital cameras suitable for the remote sensing of vegetation. In this context, monitoring the in-field variability of maize (*Zea mays* L.), characterized by high nitrogen fertilization rates, with a low-cost color-infrared airborne system could be the basis for a site-specific nitrogen (N) fertilization support system. An experimental field with different N treatments applied to silage maize was monitored during the years 2014 and 2015. Images of the field and reference destructive measurements of above ground biomass (AGB), N concentration in AGB and N uptake were taken at V6 and V9 development stages. Classical normalized difference indices and the indices adjusted by crop ground cover were calculated and regressed against the measured variables. Finally, image colorgrams were used to build PLS regression models to explore the potential of band-related information in variable estimation. The best predictors were found to be the ground cover and the adjusted GNDVI: regression equation at V9 resulted in R^2 of 0.7 and RRMSE<25% in external validation. Colorgrams did not improve prediction performances due to the spectral limitations of the camera. Therefore, the feasibility of the method should be tested in future research. In spite of limitations of sensor setup, the modified camera was able to estimate maize AGB due to the very high spatial resolution. Since AGB is a robust proxy of N status, the modified camera could be a promising tool for a low-cost N fertilization support system.

INTRODUCTION

Efficient use of agronomic inputs represents an answer to the increasing attention of public opinion to agriculture intended as a source of environmental pollution, especially referring to nitrogen (N) fertilization that could cause severe air and water pollution with environmental drawbacks (Olfs et al., 2005). A more efficient preservation of resources in agriculture can be gained by modulating external inputs according to the variability in crop response within fields. Both between- and within-field variability can be evidenced with maps describing crop status. Maps could be obtained as outputs of proximal (tractor-mounted) and remote-sensing techniques adopting optical sensors and then used to interpret dynamics of plant N demand during crop growing season, rapidly and accurately substituting destructive and time-consuming ground plant sampling and analytical measurements (Olfs et al., 2005).

Different satellite-mounted sensors are suitable for monitoring crop N status, providing information at different level of spatial (pixels from 1000 to 0.5 m) and temporal (every 1-44 days) resolution (Mulla, 2013). They usually acquire crop spectral information in the visible (VIS) and near infra-red (NIR) regions of the spectrum allowing calculating common vegetation indices. However, images require post-processing for atmospheric and geometric correction prior vegetation indices calculation (Bastiaanssen et al., 2000). Furthermore, some authors have underlined the limited operational flexibility of such techniques for real time field monitoring or management, due to low spatial resolution of acquired images, long satellite re-visit times, cloud cover and total cost of the service (Berni et al., 2009; Swain et al., 2007). However, nowadays, the improvements of satellite spatial and temporal resolution and the availability of free images renewed the interest in satellite remote sensing for agricultural purposes applied to large surfaces even if the cloud cover is still an issue due to the limited field surfaces and the limited time window suitable for field operations.

The limitations of satellite-based crop monitoring have allowed the development and spread of tractor-mounted proximal sensors. These sensors acquire reflectance at two to twenty wavebands in the vegetation indices and NIR range of the spectrum and have their own light source to avoid sunlight dependence. Moreover, tractor-based vegetation indices are used in combination with an N-rich reference filed strip that allows correcting the spectral response to local variables (Raun et al., 2008).

Besides the satellite- and tractor-mounted optical sensors, in recent years, new opportunities for crop monitoring were opened by the innovative use of unmanned aerial vehicles (UAVs). These devices, equipped with multispectral digital cameras, can be used to periodically fly over fields and acquire crop spectral information in the VIS and NIR regions in order to calculate vegetation indices at very high spatial resolution (often less than 2 cm). Recent attempts to build crop-specific calibration curves between UAV-derived vegetation indices and crop variables are recorded in the literature (Geipel et al., 2016; Huang et al., 2010; Lebourgeois et al., 2008). In fact, UAVs are more flexible in scheduling field surveys compared to satellite- and tractor- based techniques, putting forward for interesting applications in the following fields: nutrient and water management, weed control, disease and pest detection, estimation of grain yield (Wójtowicz et al., 2016). However, the ability of UAV-mounted sensors to assess vegetation status hangs on images calibration and processing that implies to retrieve reflectance, to compensate for ambient light variation (Kim et al., 2008; Noh et al., 2005), and to manage soil background noise (Noh et al, 2005). Nevertheless, UAV-based vegetation indices were successfully regressed against leaf chlorophyll concentration (R^2>0.7; Lebourgeois et al., 2008; Miao et al., 2009; Noh and Zhang, 2012), above ground biomass (R^2=0.70-0.85; Geipel et al., 2016; Reyniers e Vrindts, 2006), plant nitrogen concentration (R^2=0.4-0.8; Geipel et al, 2016; Lebourgeois et al., 2012; Reyners e Vrindts, 2006) and grain yield (R^2>0.7; Huang et al., 2010) of different crops.

Maize (*Zea mays*, L.) is the main crop cultivated in the Po plain, Northern Italy, on a surface of 327,632 ha (in Lombardy), with an average production of 11 and 50 t ha^{-1} of grain and silage-maize, respectively (ISTAT, 2017). Most of the cultivation territory of maize was classified as vulnerable to nitrate leaching (Acutis et al., 2014), and therefore loads of livestock N is limited to 170 kg N ha^{-1} year^{-1}, while, according to regional legislation, the maximum amount of N that can be annually supplied to maize (including mineral fertilizers) is 280 kg N ha^{-1} year^{-1}. Therefore, the application of UAV-based crop monitoring at high spatial and temporal resolution, with the aim of mapping crop variability linked to N nutrition, would be crucial to support site-specific fertilization and optimize fertilizer distribution, both in terms of amounts and location. This kind of monitoring is particular interesting since side-dress and top-dress fertilization of maize is applied in a narrow time window, between V6 and V9 development stages. The relative short period suggests adopting UAV-based monitoring tools rather than satellites.

Focusing on maize UAV-based monitoring, the survey of literature highlighted that only few experiments were conducted studying the behavior of a low-cost camera for the estimation of maize ground-measured variables. Different authors agreed in finding green band-based vegetation indices as the best predictors for the studied nitrogen-related variables (Osborne et al., 2004; Sakamoto et al., 2012a and 2012b; Rorie et al., 2011a and 2011b). The coefficients of determination ranged between 0.5-0.98 for the estimation of the above ground biomass (AGB), 0.49-0.7 for the estimation of AGB N concentration (Nc) and 0.38-0.59 for the estimation of N uptake (Nu). Furthermore, it must be considered that these experiences were often carried out for one or two years and often at late crop development stages (V13-R6; Ritchie et al., 1993), far from those identified as the best time window for N side-dress fertilization (V6-V9). Finally, even if V6 and V9 development stages were sensed, regression analysis was not performed specifically for those stages but comprehensive of vegetative and reproductive stages, that is including samples taken after maize flowering (Osborne et al., 2004; Sakamoto et al., 2012a and 2012b).

In the cited experiments, few vegetation indices were used to predict crop variables because sensors mounted on UAVs rarely acquired more than three broad bands. However, the most recent image analysis techniques allow expanding band-related information to be used as multivariate predictors of target features. An example is represented by the technique of colorgram extraction that was designed and implemented for food systems by Antonelli et al. (2004) to evaluate food color and defects by multivariate image analysis. It was developed for laboratory applications (Antonelli et al., 2004; Ulrici et al., 2012) and it consisted in the extraction of different color features by deriving new descriptors from the original image, and by projecting them into principal component space. Unluckily, the presented approach has never been used to extract vegetation/canopy signals from aerial images to be used as multivariate predictors of crop variables. If satisfactory, as laboratory applications suggest (Antonelli et al., 2004; Ulrici et al., 2012), this new method would allow deriving information from crop images in a fast, effective and unsupervised way. Colorgrams could be therefore an answer to the main challenge of UAV-based crop monitoring: having fast and reliable image analysis and interpretation (Rasmussen et al., 2016). In this context, such a technique is a very interesting application, especially suited to exploit the potential of band-related information recorded by a low-cost imaging system.

We present here a two years-case study where a consumer digital camera, modified to detect a NIR band and mounted on board a UAV, was used to estimate maize AGB, Nc and Nu. To this end, an experimental field with an induced fertilization gradient was used to test the opportunities and limitations of low-cost technology following three strategies. A classical strategy dealt with the calculation of common normalized difference VIs, the Green Normalized Difference Vegetation Index and the Blue Normalized Difference Vegetation Index (GNDVI and BNDVI). The second strategy first considered the estimation of the ground cover (GC), representing the fraction of soil covered by plants. Thereafter two new indices, the $BNDVI_{adj}$ and $GNDVI_{adj}$ were calculated combining the signals coming from pixels belonging to vegetation and the value of GC. In this way, indices adjusted by the GC emphasize the contribution of vegetation both in terms of reflected radiation (they do not consider pixels from soil) and soil coverage. The third strategy involved the extraction of colorgram signals from multispectral images of the field (soil plus vegetation) and of the solely vegetation. Finally, linear and multivariate partial least square (PLS) regression models were applied to estimate maize variables from vegetation indices and colorgrams, respectively. Therefore, based on regression model performances, we tested whether the modified camera could be used to provide low-cost advices for maize N fertilization.

MATHERIALS AND METHODS

The UAV survey was carried out on a flat field located in Montanaso Lombardo (Lodi), Italy (45°20'32" N, 9°26'43" E, altitude 80 m asl) during 2014 and 2015 maize growing seasons. The field hosted a multi-year experiment (Cavalli et al., 2014 and 2016) aimed at quantifying N use efficiency of livestock manures applied to silage-maize (Hybrid PR33M15, Pioneer Hi-Bred Italia S.r.l.) followed by an unfertilized catch crop of Italian Ryegrass (*Lolium perenne*, Lam. Cv Asso). The trial started in spring 2011 and comprised the following six treatments: 1) unfertilised control (CON); 2) ammonium sulphate (AS); 3) unseparated digestate from a mix of cattle slurry and maize (DSMM); 4-5) the liquid (LF) and solid (SF) fractions of DSMM; 6) unseparated anaerobically stored cattle slurry (US).

Treatments were applied on plots of 112.5 m^2 (15 m long and 7.5 m wide) and were arranged in a randomized block design with four replicates (plots 1-24 in Figure 1). Blocks were separated each other by ten meters strips. Every year, from 2011 to 2014, manures and AS were applied to the same plots at similar NH_4-N rates (on average 140 kg NH_4-N ha^{-1}). Differences in applied organic N and in N use efficiency among fertilizers provided a wide range of variability in plant available N within the field. For this reason, the field was chosen to be surveyed by the UAV mounting the modified camera, for calibration purposes. In spring 2015 fertilizations were suspended in order to quantify residual N effects of previous fertilizations (Cavalli et al., 2016). An additional treatment of ammonium sulphate (AS_{150}; 150 kg N ha^{-1}) was applied in half of the original AS plots in order to compare apparent N recovery of 2014 with that of previous years (plots 25-28 in Figure 1). Furthermore, three other treatments of mineral fertilizers were added to the original design to rise further variability of plant available N. Additional treatments comprised ammonium sulphate applied at 35 and 70 kg N ha^{-1} (AS_{35} and AS_{70}), and calcium nitrate applied at a rate of 150 kg N ha^{-1} (CAN_{150}). They were applied on plots of 60 m^2 (8 m long and 7.5 m wide) arranged in a randomized block design with four replicates, and located in the strips between blocks of the original experiment (plots 29-40 in Figure 1). Finally, during 2015, eight unfertilized areas of about 1.5 m^2 outside the experimental plots were sampled in order to further increase variability in the collected samples (points 41-48 in Figure 1).

FIGURE 1, HERE.

Crop sampling and analysis

Plants were sampled at maize phenological stages V6 and V9 (six and nine fully expanded leaves; Ritchie et al., 1993) in both years, corresponding to 18 July and 1 August 2014 and 3 July and 13 July 2015, respectively. Aboveground biomass (AGB) was estimated by collecting 15 whole plants per plot (three plants per row of the five inner rows of each plot). Plants were oven dried (105°C) until constant weight in order obtain AGB values on a dry matter (DM) basis. Samples were ground with a ZM 100 centrifugal mill equipped with a sieve of 0.2 mm mesh (Retsch Gmbh & Co., Haan, Germany). Total nitrogen concentration in AGB (Nc; g N 100 g DM^{-1}) was determined by dry combustion using a ThermoQuest NA1500 elemental analyser (Carlo Erba, Milano, Italy). Nitrogen uptake of maize (Nu; g N m^{-2}) was calculated by multiplying AGB (g DM m^{-2}) by Nc.

Image acquisition and processing

A consumer digital camera Canon® Powershot SX260 HS was converted to a color-infrared camera (CIR) by removing the infrared blocking filter and adding a Super Blue IR filter (www.publiclab.com). Therefore, the red channel was used to acquire reflectance in the NIR, while the blue (B) and green (G) channels remained the same. After the modification, the spectral resolution of the camera was tested in laboratory conditions by single waveband measurements in the range between 400 and 800 nm, every 10 nm using a monochromator equipped with a Xenon lamp. Images were acquired in a dark room, at a distance of 7 cm from the light source, with the monochromatic ray normally striking the camera sensor. The camera was manually set up to eliminate saturated values in any band using the following settings: focus, 8.0, exposure time 1/60 s and sensitivity ISO100.

The CIR camera was mounted on board a prototype UAV coaxial octocopter. The UAV was made of carbon fiber with a maximum payload of 12 kg and was equipped with a GNSS (Global Navigation Satellite System) NEO-M8N (u-blox, Thalwil, Switzerland) and double gimbal platform for mounting the camera.

Images were acquired immediately before plant sampling, under clear sky conditions, between 11:00 and 13:00 a.m. solar time, assuring no variation in the incident light angle, and under homogeneous soil wetness level. The UAV survived the field at a speed of 5 m s^{-1} and an altitude of 35 m above ground level. The flight plan guaranteed a 75% forward and sideward overlap between images.

Images were recorded in 8-bit JPEG format with the camera pointing to the nadir direction. The JPEG file format was chosen because JPEG file dimensions were more feasible for UAV-applications at farmer level. Furthermore, geometric and vignetting corrections were done by the original Canon firmware. The camera was set up with autofocus mode, maximum wide angle, a fixed ISO value of 200, 1/1250 s shutter speed. The automatic aperture stop resulted to be the same each flight (3.625) due to the short flight duration time and optimal light conditions. The output images were 12.1 MP (Mega pixel), 3-band 8-bit per band JPEG files, with a spatial resolution of 1.5 cm. Orthomosaics of the images were made, separately for each day of acquisition, using the software Pix4Dmapper (Pix4D SA, Lausanne, Switzerland) that performed a 3D points-based stitching. No radiometric calibration was carried out at this step. Areas belonging to ground points were extracted from orthomosaics, obtaining images representative of the sampled areas of the field. In the year 2014 and 2015, the area corresponding to the inner five rows of each plot was extracted. In addition, areas corresponding to points 41-48 was selected close to ground sample using GPS coordinates as reference. Thus, given the different size of some plots in 2014 and 2015 and that of additional points out of plots, extracted images had different size. A white tile positioned in each plots was used to calculate the reflectance values of the images, by normalizing pixel intensities by the value of the white reference, after subtracting the black reference. Black reference consisted by sampling the lowest intensity value recorded by all the images of the same flight.

Vegetation indices

The Blue Normalized Difference Vegetation Index (BNDVI) and the Green Normalized Difference Vegetation Index (GNDVI) were calculated, for each pixel of extracted images according to the following equations:

$$\text{Classical NDVI-based indices} = \frac{\text{NIR-Band}}{\text{NIR+Band}} \qquad \textit{Eq. 1}$$

Were Band stands for the blue band in the case of BNDVI and green band in the case of GNDVI. Indices were calculated using MATLAB version R2014b (MathWorks, Natick, MA).

The Otsu algorithm (Otsu, 1975) was used to identify, within each image, pixels belonging to vegetation. Segmentation was based on BNDVI or GNDVI providing, in both cases, a mask of the vegetation ($Mask_{veg}$). The BNDVI-based segmentation strategy resulted in a better separation between soil and vegetation, while GNDVI did not discriminate soil shadows from leaves, resulting in undersegmentation. Therefore, the canopy ground cover (GC), representing the fraction of total pixels classified as vegetation, was calculated using $Mask_{veg}$ based on BNDVI.

After GC calculation, two additional indices were derived from BNDVI and GNDVI in order to give a zero weight to pixels classified as soil, and thus emphasize the signal coming from vegetation. The two indices, $BNDVI_{adj}$ and $GNDVI_{adj}$, were calculated using following the equation:

$$VI_{adj} = \frac{\sum_{i=1}^{n}\sum_{j=1}^{m} VI_{ij} \times Mask_{veg\ ij}}{\sum_{i=1}^{n}\sum_{j=1}^{m} Mask_{veg\ ij}} \times GC \qquad \textit{Eq. 2}$$

where VI_{ij} and $Mask_{veg\ ij}$ are the value of the vegetation index (BNDVI or GNDVI) and the classification value (zero or one) of the pixel *ij*, respectively, while *n* and *m* represent the number of rows and columns of the image. For both indices, the classification mask $Mask_{veg}$ was based on BNDVI values.

Image colorgrams

Colorgrams were constructed following the method proposed by Antonelli et al. (2004) with the aim of extracting the most complete information related to image color. Each colorgram is a linear signal that sequentially combines frequency distributions of the following band-related information: 1) intensity values of the three channels NIR, G, and B (region 1-768); 2) lightness, calculated as the sum of the three channels intensities (region 769-1024); 3) relative channel intensities, calculated as the ratio between channel intensity and lightness (region 1025-1792); 4) values of the original channels after projection in the hue space (region 1793-2560). Finally, scores values derived from a three-PCA model applied to the image are calculated and joined to the colorgram signal (region 2561-4864). The model is applied on the raw, the mean centered and the autoscaled spectra matrices because the process is unsupervised, without any prior knowledge on which pretreatment performs better than others (Antonelli et al., 2004). Loadings and eigenvalues, derived from the PCA model, are added as the final part of the signal (region 4865-4900). In this work, we introduced a standardization procedure not used in the original paper. The frequency distributions forming each colorgram were divided by the number of pixels of each image. In the original method (Antonelli et al., 2004) no standardization was required because images had the same dimensions, however, in this work, we worked on both full and segmented images (i.e. considering only pixels classified as vegetation). Therefore, the number of pixels used in the procedure differed among images, and standardization was needed.

Standardized colograms of whole images (CLRG) and segmented images ($CLRG_{veg}$) were built using MATLAB and an ad-hoc self-built function. Figure 3 shows the resulting signals.

Statistical analysis

Analysis of variance (ANOVA) was carried out, separately for each year and sampling date, to test the significant effect of treatment on AGB, GC and $GNDVI_{adj}$. The ANOVA model considered the treatment as a fixed factor and block as random. The homogeneity of variances was evaluated using the Levene test (P<0.05). Significant effects of treatments are reported when the P is below 0.05. Treatments were grouped according to the HSD Tukey test (P<0.05). All ANOVAs were performed using the SPSS procedure UNIANOVA (SPSS Versions 24.0.0).

The aim of mean separation was to evaluate whether treatments statistically affected measured variables and vegetation indices in a similar way. Therefore, we were interested in assessing if vegetation indices could be able to discriminate among statistically different means of measured variables originated from different available N rates (originating from both yearly added N fertilizers or mineralized residual organic N).

Linear regression models were built, separately for each crop development stage V6 and V9, to estimate AGB, Nc and Nu from the six predictors: BNDVI and GNDVI, GC based on BNDVI and GNDVI, and indices $BNDVI_{adj}$ and $GNDVI_{adj}$.

Multivariate analysis was used to predict AGB, Nc and Nu from standardized colorgrams. Partial least square regression models (PLS) were built, separately for V6 and V9, using CLGR or $CLGR_{veg}$ colorgrams.

The entire dataset (24 and 48 sampling points for 2014 and 2015, respectively) was divided into a calibration and a validation dataset. The calibration dataset (48 samples) comprised all samples from the 2014 campaign (24 samples) and samples from the 2015 campaign belonging to plots 27-40 and sampling points 41-48 (24 samples). The remaining

24 samples of the year 2015 were used as validation datasets. The resulting datasets partially minimized the occurrence of autocorrelation between samples taken on the same plot in the two consecutive years.

Finally, linear and PLS regressions models were built on the pooled data of the two phenological stages by joining the dataset of V6 and V9, resulting in a global dataset of 96 and 48 samples for calibration and validation, respectively. These models provided prediction of maize variables for a time window suitable for side-dress N fertilization.

The statistics coefficient of determination (R^2) and relative root mean squared error (RRMSE; %) were used to judge the performances of linear and PLS regression models, both applied to the calibration and validation datasets.

RESULTS

Camera sensitivity

FIGURE 2, HERE.

Sensitivity test on the CIR camera showed that the blue channel had a peak at 460-490 nm, centered at the blue wavelengths of 460 nm. However, blue pixels acquired also wavelengths from 400 to 560 nm, covering part of the green region of the visible spectrum. The green channel resulted narrower than the blue one and it was sensible to the wavelengths from 470 to 570 nm with a peak on the green region (540-550 nm). Finally, the red channel, after modification, recorded the NIR wavelengths going from 680 to 800 nm. The removal of the NIR filter caused the overlapping of the three channels in the NIR region: in fact, also the blue and the green channel recorded wavelengths from 680 to 800 nm. The NIR channel, finally, acquired a small portion of the visible light in the blue and green regions of the spectrum due to the applied superblue filter.

Measured datasets

During each season, maize AGB and Nu markedly increased from V6 to V9 (Table 1), while N in AGB tissues was progressively diluted, as confirmed by lower Nc values at V9 compared to V6 (Table 1). Variability of measured variables was narrow at V6, and it was similar for the years 2014 and 2015, suggesting that fertilizer N effects occurred at later stages of crop development in both years. Indeed, despite variable applied N fertilization levels, only few significant differences ($P<0.05$; Table 1) in AGB and Nu were found among treatments. In particular, AGB was higher in SF compared to CON, AS and DSMM in 2014, while in 2015, only SF and chemical fertilizers added at a rate of 150 kg N ha^{-1} (AS_{150} and CAN_{150}) significantly enhanced maize AGB compared to CON. A similar pattern was observed for Nu and Nc in 2015, while in 2014 Nc did not significantly varied among treatments.

Conversely, when crop reached V9, higher variability was measured in 2015 than in 2014, in agreement with the wider range of applied N rates. ANOVA confirmed that treatments in 2015 significantly ($P<0.05$) affected both crop biomass and Nu (Table 1). Conversely, maize did not responded significantly to N fertilization in 2014, when all treatments showed similar AGB and Nu.

TABLE 1, HERE.

Vegetation indices

Vegetation indices, both classical (BNDVI and GNDVI) and adjusteded ($BNDVI_{adj}$ and $GNDVI_{adj}$), and GC increased during crop development from V6 to V9, according to the increase in AGB and plant N uptake (Table 1).

In general, the effect of treatments on vegetation indices and GC was similarly to that on AGB and Nu, as confirmed by homogeneous groups reported in Table 1. However, at V6 in 2015, grouping based on vegetation indices and GC did not differentiate between treatments receiving fertilizers at a rate of 150 kg N ha^{-1} and CON, as grouping for AGB and Nu suggested.

At V9, all indices showed a relationship with AGB characterized by a linear response followed by a flat response, suggesting a saturation of the blue and green channels at high AGB levels (Figure 3 for GNDVI and $GNDVI_{adj}$). Optimization of a simple linear-plateau model confirmed that lack of response occurred at AGB levels higher than 220 g DM m^{-2}.

Correction of BNDVI and GNDVI by GC allowed increasing the slope of the relations between the indices and AGB, and increasing the value of the plateau by about 10% compared to corresponding uncorrected indices, and thus to extent the linear relationship (Figure 3).

Linear PLS Regression models

Division of collected data into a calibration and a validation dataset provided sufficient variability in measured variables in both generated sets (Table 2). In addition, the validation sets were always included into calibration limits, ensuring to respect the domain of applicability of the calibrated models.

Regressions between vegetation indices and Nc were not significant at both phenological stages (Table 3). The lack of a strong biochemical relationship between the broad bands collected by the CIR camera and Nc resulted in poor calibration models when the range of variation explored by the measured data was not wide enough. Indeed, joining the datasets of the two phenological stages (V6+V9) enabled improving calibration performances, obtaining significant regression models and acceptable validation errors (RRMSE <18%). Even if similar calibration performances were found among all the tested indices, those adjusted by the GC gave better results in validation, without visible difference among GC, $BNDVI_{adj}$ and $GNDVI_{adj}$. The fact that Nc was successfully estimated due to the effect of nitrogen treatments on AGB and not thanks to the different levels of greenness recorded by the camera was confirmed by the similar results in the external validation between vegetation indices and colorgrams (Table 3).

TABLE 2 AND 3, HERE.

The calibrated regression models for the estimation of Nu at V6 gave poor results (R^2<0.2), probably due to the low capability of the camera in recording low AGB levels at early development stages. In fact, also AGB estimation gave poor results at V6 (Table 3). The good performances in calibration shown by the PLS regression models built using colorgrams as AGB predictors seemed contradictory. In fact, very high coefficients of determination (R^2>0.8) and

RRMSEs less than 10% were obtained in calibration. Despite these good results, in the external validation (R^2<0.5 and RRMSE ~ 20%) the PLS models based on colorograms proved not to be robust.

Very satisfactory results were found in AGB estimations performed at V9. Similar performances were found among classical vegetation indices and the indices adjusted by the GC in terms of R^2 and RRMSE of calibration: 0.85 and 17.5% on average, respectively. PLS regression models built on colorgrams led to slightly better results in calibration. The similar performances of the colorgrams of the entire image and of vegetation only were expected, because at V9 the contribution of soil pixels to the canopy signal was minimal due to the high GC of maize canopy. External validation proved that models based on GC and indices adjusted for the vegetation fraction were very similar to each other and the best performing (in particular GC and $GNDVI_{adj}$) compared to the classical vegetation indices (Figure 3), BNDVI and GNDVI, and colorgrams.

Finally, the best results were found when the V6 and V9 datasets were joined. The high variability explored (Table 2) led to the best calibration models for all the tested indices. The higher sensibility of the indices to the variation of AGB levels was confirmed and Nc estimation greatly improved.

FIGURE 3, HERE.

DISCUSSION

At first, the spectral response of the camera after the modification was studied. This step was needed in order to understand the feasibility of the camera for crop monitoring in terms of accuracy of the band-related information acquired by the sensor. In agreement with previous studies on modified digital cameras (Pauly, 2014 and 2016) it was found out that the CIR camera suffered of channel overlapping (Figure 2). This caused the resulting channel intensities to be correlated and therefore, band-related information, as acquired by the CIR camera, was not the most relevant feature at the basis of the capacity of the camera to discriminate among different AGB, Nc and Nu levels. Indeed, PLS models built using colorgrams as predictors of AGB, Nc and Nu, even with good calibration performances, did not improve validation performances compared to classical vegetation indices and to indices adjusted by GC (Table 3). This result supported the hypothesis that features of the camera other than band-related information mostly contributed to maize variable predictions (Table 3), since colorgrams were thought as a technique to extract redundant band-related information (Antonelli et al., 2004). Indeed, the ability of the image-based vegetation indices to assess vegetation status relied on the strong relationship existing between the indices and canopy GC that was related, in turn, to AGB (Hunt et al., 2010; Li et al., 2010; Zhou et al., 2018), at least in early stages of crop development. Imaging sensors basically acquire information about soil coverage by canopy: as GC increases, the portion of vegetation pixels increases until canopy closure (that usually occurs after V9, in maize). Thus, in the time window from emergence to canopy closure, very high spatial resolution imagery could play a role in the assessment of AGB variability even if the sensors used are characterized by low radiometric resolution and overlapping channels.

In this context, the difficult estimation of Nc at V6 and V9 (Table 1 and 3) was expected because vegetation indices were known to be affected by the confounding effects of changings of canopy architecture (Eitel et al., 2008). Moreover, our best results, obtained by combining data of V6 and V9 (Table 3), were similar to those obtained in comparable experiments on maize conducted with airborne multispectral imagery (Osborne et al., 2004; Vergara-Dìaz et al., 2016). In both cited experiments, linear regression models to predict Nc based on GNDVI performed better than those based on red NDVI, and provided similar prediction performances in the two experiments (R^2 0.23-0.49) when maize was at phenological stages V14-R1 (flowering). The lack of channel signal accuracy of the CIR camera used in our experiment was probably balanced by the high range of variation of the measured Nc (1.69-4.07% for the V6+V9 dataset; Table 2) that allowed gaining similar performances.

As expected, estimation of AGB gave the best results while the goodness of Nu estimation depended on the performances in the estimation of both, AGB and Nc. Therefore, we will focus our discussion on AGB estimation. The ANOVA highlighted that differences in AGB among treatments were sensed by all indices quite well (Table 1), irrespective to the saturation phenomenon that probably affected the vegetation index at high AGB levels (Figure 3). The fact that treatment groups based on measured maize variable and vegetation indices agreed, together with prediction performances for the V9 and V6+V9 datasets (Table 3) led to the conclusion that the modified digital camera could be a valuable tool in identifying the within-field variability of maize in the time window from V6 to V9, suitable for N fertilization.

However, results at V6 suffered from problems of image acquisition in the 2015 campaign. Indeed, the 2015 dataset, that constituted part of the calibration dataset (Figure 3), was characterized by a narrow variation in GC (0.19-0.23) against a wide range of measured AGB (28-55 g DM m^{-2}). Therefore, the error in the estimation of AGB was probably due to some blurred images collected during the 2015 survey, as confirmed by individually visual inspection of acquired images. These images prevented the algorithm of segmentation working properly and maize plants resulted oversegmented and consequently, the GC underestimated. Another issue that could have played a role is the correlation observed among the collected bands (Figure 2). Pauly (2016) noted that it caused a more difficult discrimination between leaves and soil when using modified cameras that are affected by channel overlapping, as in this case. The described factors probably affected the estimation performances at V6, where the confounding effects of soil and shadows were higher than at V9 (Sripada et al., 2005). An example of the segmentation procedure is provided in figure 4. This reason could explain the low performances at V6 of the indices and, in particular, the worse performance of the GC and of the adjusted indices if compared to the classical BNDVI and GNDVI that were not affected by the segmentation procedure.

FIGURE 4, HERE.

The most satisfactory results were obtained at V9. Indeed, good quality images in both years guaranteed the extraction of reliable vegetation indices; in addition, the high range of the measured AGB at V9 was markedly suited for calibration purposes. High R^2 (0.68-0.71; Table 3) and low RRMSE (22-24%) were gained in validation for GC and adjusted indices $BNDVI_{adj}$ and $GNDVI_{adj}$. The better performances of GC and of the adjusted indices could be explained by the fact that the GC had a more linear response to AGB than the classical indices themselves (Figure 3). Therefore, the use of GC as a weighting factor allowed linearizing responses of the vegetation indices to the AGB levels. Accordingly, the distributions of the indices weighted for GC were more similar to the distribution of AGB values and less affected by saturation: GNDVI saturated at 234 g DM m^{-2} while $GNDVI_{adj}$ saturated at 250 g DM m^{-2}, similarly to GC. Our results in AGB estimation were very positive compared to those found in multispectral imagery-based experiments on maize, even done with airborne sensors specific for vegetation monitoring: 0.18-0.65 of R^2 (Osborne et al., 2004) *vs* 0.80-0.88 of our experiment. Finally, experiments with digital camera mounted on ground stations (Sakamoto et al., 2012a and 2012b) gave comparable results (R^2=0.79-0.99 obtained by non-linear fitting and by vegetation indices other than NDVI and GNDVI). The better results could be ascribed to the wide window of the explored maize development stages (the entire season), to the good quality of the images, more manageable form a ground station compared to airborne sensors, to the quality of the camera spectral response and to the different fitting methods and vegetation indices studied. None of the cited literature gave information about performance in validation of the proposed equations. Even in the cases of models based on indices acquired with hyperspectral imaging sensors characterized by high spectral and radiometric resolution (Cilia et al., 2014; Perry and Roberts, 2008), calibration results were from worse to comparable with R^2 of 0.45 (V14) and 0.77 (V10). The fact that the estimation of AGB was reliable and comparable to those obtained with more refined approaches, confirmed the promising results of the proposed method, in spite of the limitations of our sensor setup. However, some aspects must be taken into account for future research to fully explore the feasibility of the use of a modified low-cost camera for maize monitoring: the time window going from V6 to V9 should be adequately investigated in order to provide a unique calibrated equation suitable for the estimation of maize AGB and Nu at the time of N fertilization. More attention should be paid for image quality in terms of absence of blurred images, a calibrated reference panel should be used to get more reliable image intensity values (Pauly, 2014) and RAW (native image file format) images acquisition should be considered (Verhoeven et al., 2010). Finally, since the colorgram-based estimations were affected by overfitting, probably due to redundancies in band-related information as acquired by the CIR camera, in future research, the feasibility of the method could be studied by testing it on ground-based images taken by an RGB camera or by a multispectral narrow-band camera, to avoid channel overlapping and the related issues. In fact, the colorgram approach that offers an unsupervised image processing for object classification and prediction of object properties could be an interesting tool for ground-based monitoring in controlled environment, more suitable to enhance the power of the band-related information.

CONCLUSION

The experiment aimed testing the potential of a low-cost consumer camera, modified into a CIR camera, to detect maize variables (AGB, Nc and Nu) as influenced by different nitrogen treatments. The CIR camera resulted to have issues related to channel overlapping and thus, correlated bands with consequences on the accuracy of the acquired band-related information. Moreover, JPEG compression reduced the tonal values of the images. However, vegetation indices were tested using one-way ANOVA, providing N treatment separation in accordance with measured variables, and thus the capability of the camera to detect the within-field variability was proved.

In order to explore the potential of the imaging sensor, colorgrams were extracted and, for the first time applied in-field vegetation monitoring. They were used as predictors of the chemical and physical properties of the canopy *via* multivariate data analysis. This new technique turned out not to be superior to linear regression models based on vegetation indices, probably due to the correlation observed among the acquired bands. In addition, colorgrams provided very good performances of calibration models at both V6 and V9 (R^2>0.8 and RRMSE<15%) but failed in estimating maize nitrogen-related variables of external validation datasets probably due to model overfitting.

The outlined issues in band acquisition (overlapping channels) could also explain the similar behavior of the common vegetation indices BNDVI and GNDVI. The best performing indices were the ones calculated using the information of the vegetation fraction, in particular GC and $GNDVI_{adj}$. In spite of camera limitations, very good performances in AGB and Nu estimation were found at V9 stage and then at V6+V9 stages, when a larger range of variation in the measured variables was explored: AGB was estimated with R^2 of 0.9 and RRMSE=25% were gained in the external validation step by $GNDVI_{adj}$. At V6+V9 stages, nitrogen concentration was estimated (external validation) with R^2 of 0.67 and RRMSE=17%, as well. Results at V6 were affected by low quality of some images and thus, in future research, the time window V6-V9 should be fully investigated to provide a calibrated equation suitable for the estimation of maize AGB and Nu at the time of N fertilization. In conclusion, the low cost imaging system, even with the limitations due to bands overlap and JPEG compression, was able to detect the within-field variability and to produce reliable estimates of maize AGB. This was possible thanks to the very high spatial resolution of the imaging sensor that allowed estimating the canopy ground cover.

REFERENCES

Acutis, M., Alfieri, L., Giussani, A., Provolo, G., Di Guardo, A., Colombini, S., Bertoncini, G., Castelnuovo, M., Sali, G., Moschini, M. (2014). ValorE: An integrated and GIS-based decision support system for livestock manure management in the Lombardy region (northern Italy). Land use policy 41, 149–162.

Antonelli, A., Cocchi, M., Fava, P., Foca, G., Franchini, G.C., Manzini, D., Ulrici, A. (2004). Automated evaluation of food colour by means of multivariate image analysis coupled to a wavelet-based classification algorithm. *Analytica Chimica Acta* 515(1), 3–13.

Bastiaanssen, W.G., Molden, D.J., Makin, I.W. (2000). Remote sensing for irrigated agriculture: examples from research and possible applications. *Agricultural water management* 46(2), 137–155.

Berni, J.A.J., Zarco-Tejada, P.J., Suárez, L., González-Dugo, V., Fereres, E. (2009). Remote sensing of vegetation from UAV platforms using lightweight multispectral and thermal imaging sensors. *The International Archives of the Photogrammetry, Remote Sensing and Spatial Information Sciences* 38(6).

Cavalli, D., Cabassi, G., Borrelli, L., Fuccella, R., Degano, L., Bechini, L., Marino, P. (2014). Nitrogen fertiliser value of digested dairy cow slurry, its liquid and solid fractions, and of dairy cow slurry. *Italian Journal of Agronomy* 9(2), 71–78.

Cavalli, D., Cabassi, G., Borrelli, L., Geromel, G., Bechini, L., Degano, L., Marino, P. (2016). Nitrogen fertilizer replacement value of undigested liquid cattle manure and digestates. *European Journal of Agronomy* 73, 34–41.

Eitel, J.U.H., Long, D.S., Gessler, P.E., Hunt, E.R. (2008). Combined Spectral Index to Improve Ground-Based Estimates of Nitrogen Status in Dryland Wheat. *Agronomy Journal* 100(6), 1694-1702. https://doi.org/10.2134/agronj2007.0362

Geipel, J., Link, J., Wirwahn, J.A., Claupein, W. (2016). A Programmable Aerial Multispectral Camera System for In-Season Crop Biomass and Nitrogen Content Estimation. *Agriculture* 6(1), 4. doi:10.3390/agriculture6010004

Huang, Y., Thomson, S.J., Lan, Y., Maas, S.J. (2010). Multispectral imaging systems for airborne remote sensing to support agricultural production management. *International Journal of Agricultural & Biological Engineering* 3(1), 50-62.

Hunt, E.R., Hively, W.D., Fujikawa, S.J., Linden, D.S., Daughtry, C.S., McCarty, G.W. (2010). Acquisition of NIR-green-blue digital photographs from unmanned aircraft for crop monitoring. *Remote Sensing* 2(1), 290–305.

Kim, Y., Reid, J.F., Zhang, Q. (2008). Fuzzy logic control of a multispectral imaging sensor for in-field plant sensing. *Computers and Electronics in Agriculture* 60(2), 279–288.

Lebourgeois, V., Bégué, A., Labbé, S., Houlès, M., Martiné, J.F. (2012). A light-weight multi-spectral aerial imaging system for nitrogen crop monitoring. *Precision agriculture* 13(5), 525–541.

Lebourgeois, V., Bégué, A., Labbé, S., Mallavan, B., Prévot, L., Roux, B. (2008). Can commercial digital cameras be used as multispectral sensors? A crop monitoring test. *Sensors* 8(11), 7300–7322.

Li, Y., Chen, D., Walker, C.N., Angus, J.F. (2010). Estimating the nitrogen status of crops using a digital camera. *Field crops research* 118(3), 221–227.

Miao, Y., Mulla, D.J., Randall, G.W., Vetsch, J.A., Vintila, R. (2009). Combining chlorophyll meter readings and high spatial resolution remote sensing images for in-season site-specific nitrogen management of corn. *Precision agriculture* 10(1), 45–62.

Mulla, D.J. (2013). Twenty five years of remote sensing in precision agriculture: Key advances and remaining knowledge gaps. *Biosystems Engineering* 114(4), 358–371.

Noh, H., Zhang, Q. (2012). Shadow effect on multi-spectral image for detection of nitrogen deficiency in corn. *Computers and Electronics in Agriculture* 83, 52–57.

Noh, H., Zhang, Q., Han, S., Shin, B., Reum, D. (2005). Dynamic calibration and image segmentation methods for multispectral imaging crop nitrogen deficiency sensors. *Transactions-American Society Of Agricultural Engineers* 48(1), 393–401.

Olfs, H.-W., Blankenau, K., Brentrup, F., Jasper, J., Link, A., Lammel, J. (2005). Soil- and plant-based nitrogen-fertilizer recommendations in arable farming. *Journal of Plant Nutrition and Soil Science* 168(4), 414–431. https://doi.org/10.1002/jpln.200520526

Osborne, S.L., Schepers, J.S., Schlemmer, M.R. (2004). Using multi-spectral imagery to evaluate corn grown under nitrogen and drought stressed conditions. *Journal of Plant Nutrition* 27(11), 1917–1929. doi:10.1081/LPLA-200030042

Otsu, N. (1979). A threshold selection method from gray-level histograms. *IEEE transactions on systems, man, and cybernetics*, 9(1), 62-66.

Pauly, K. (2014). Applying conventional vegetation vigor indices to UAS-derived orthomosaics: issues and considerations. *Proceedings of the 12th International Conference for Precision Agriculture*, Sacramento, California, USA.

Pauly, K. (2016). Towards Calibrated Vegetation Indices from UAS-derived Orthomosaics. *Proceedings of the 13th International Conference for Precision Agriculture*, St. Louis, Missouri, USA.

Rasmussen, J., Ntakos, G., Nielsen, J., Svensgaard, J., Poulsen, R.N., Christensen, S. (2016). Are vegetation indices derived from consumer-grade cameras mounted on UAVs sufficiently reliable for assessing experimental plots? *European Journal of Agronomy* 74, 75–92.

Raun, W.R., Solie, J.B., Taylor, R.K., Arnall, D.B., Mack, C.J., Edmonds, D.E. (2008). Ramp Calibration Strip Technology for Determining Midseason Nitrogen Rates in Corn and Wheat. *Agronomy Journal* 100(4), 1088–1093. https://doi.org/10.2134/agronj2007.0288N

Reyniers, M., Vrindts, E. (2006). Measuring wheat nitrogen status from space and ground- based platform. *International Journal of Remote Sensing* 27(3), 549–567. doi:10.1080/01431160500117907

Ritchie, S.W., J.J. Hanway, and G.O. Benson. (1993). How a corn plant develops. Rev. ed. Spec. Rep. 53. Iowa State Univ. Coop. Ext. Serv., Ames.

Rorie, R.L., Purcell, L.C., Karcher, D.E., King, C.A. (2011a). The Assessment of Leaf Nitrogen in Corn from Digital Images. *Crop Science* 51(5), 2174–2180. doi:10.2135/cropsci2010.12.0699

Rorie, R.L., Purcell, L.C., Mozaffari, M., Karcher, D.E., King, C.A., Marsh, M.C., Longer, D.E. (2011b). Association of “Greenness” in Corn with Yield and Leaf Nitrogen Concentration. *Agronomy Journal* 103(2), 529. doi:10.2134/agronj2010.0296

Sakamoto, T., Gitelson, A.A., Nguy-Robertson, A.L., Arkebauer, T.J., Wardlow, B.D., Suyker, A.E., Verma, S.B., Shibayama, M. (2012a). An alternative method using digital cameras for continuous monitoring of crop status. *Agricultural and Forest Meteorology* 154, 113–126.

Sakamoto, T., Gitelson, A.A., Wardlow, B.D., Arkebauer, T.J., Verma, S.B., Suyker, A.E., Shibayama, M. (2012b). Application of day and night digital photographs for estimating maize biophysical characteristics. *Precision Agriculture* 13(3), 285–301. doi:10.1007/s11119-011-9246-1

Sripada, R.P., Heiniger, R.W., White, J.G., Weisz, R. (2005). Aerial color infrared photography for determining late-season nitrogen requirements in corn. *Agronomy Journal* 97(5), 1443–1451.

Swain, K.C., Jayasuriya, H.P.W., Salokhe, V.M. (2007). Low-altitude remote sensing with unmanned radio-controlled helicopter platforms: A potential substitution to satellite-based systems for precision agriculture adoption under farming conditions in developing countries. *International Commission of Agricultural Engineering*, Vol.9.

Ulrici, A., Foca, G., Ielo, M.C., Volpelli, L.A., Fiego, D.P.L. (2012). Automated identification and visualization of food defects using RGB imaging: Application to the detection of red skin defect of raw hams. *Innovative Food Science & Emerging Technologies* 16, 417–426.

Vergara-Díaz, O., Zaman-Allah, M.A., Masuka, B., Hornero, A., Zarco-Tejada, P., Prasanna, B.M., Cairns, J.E., Araus, J.L. (2016). A novel remote sensing approach for prediction of maize yield under different conditions of nitrogen fertilization. *Frontiers in plant science* 7, 666.

Verhoeven, G.J.J. (2010). It's all about the format–unleashing the power of RAW aerial photography. *International Journal of Remote Sensing* 31(8), 2009–2042.

Wójtowicz, M., Wójtowicz, A., Piekarczyk, J. (2016). Application of remote sensing methods in agriculture. *Communications in Biometry and Crop Science* 11, 31–50.

Zhou, Z., Jabloun, M., Plauborg, F., Andersen, M.N. (2018). Using ground-based spectral reflectance sensors and photography to estimate shoot N concentration and dry matter of potato. *Computers and Electronics in Agriculture* 144, 154–163.

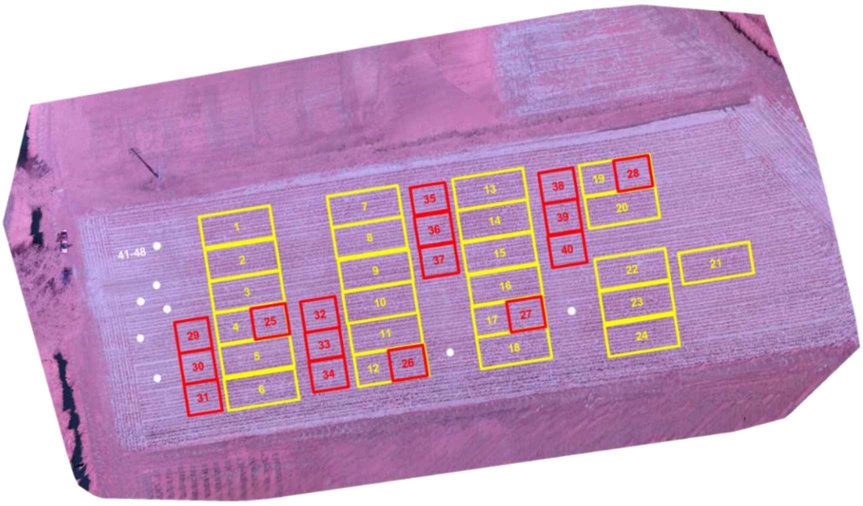

Figure 1. – Aerial orthomosaic of the field acquired at 18 July 2014 (maize at V6 stage). Plots 1-24: original experimental design (sampled in 2014 and 2015); plots 25-40: additional N treatments (sampled only in 2015); points 41-48: additional 2015 sampling points.

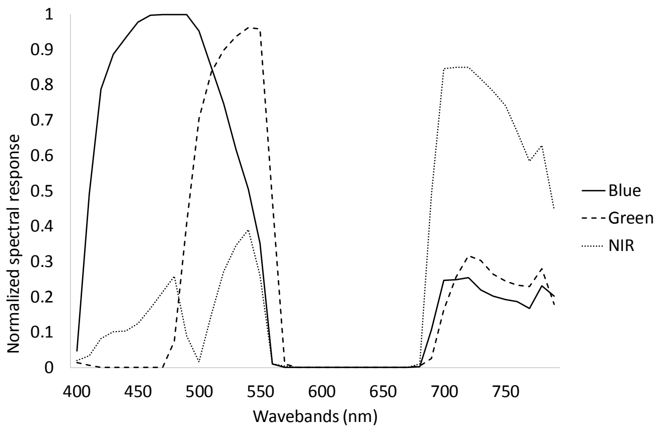

Figure 2. – Spectral sensitivity of the three channels of the modified Canon Powershot SX260 HS digital camera.

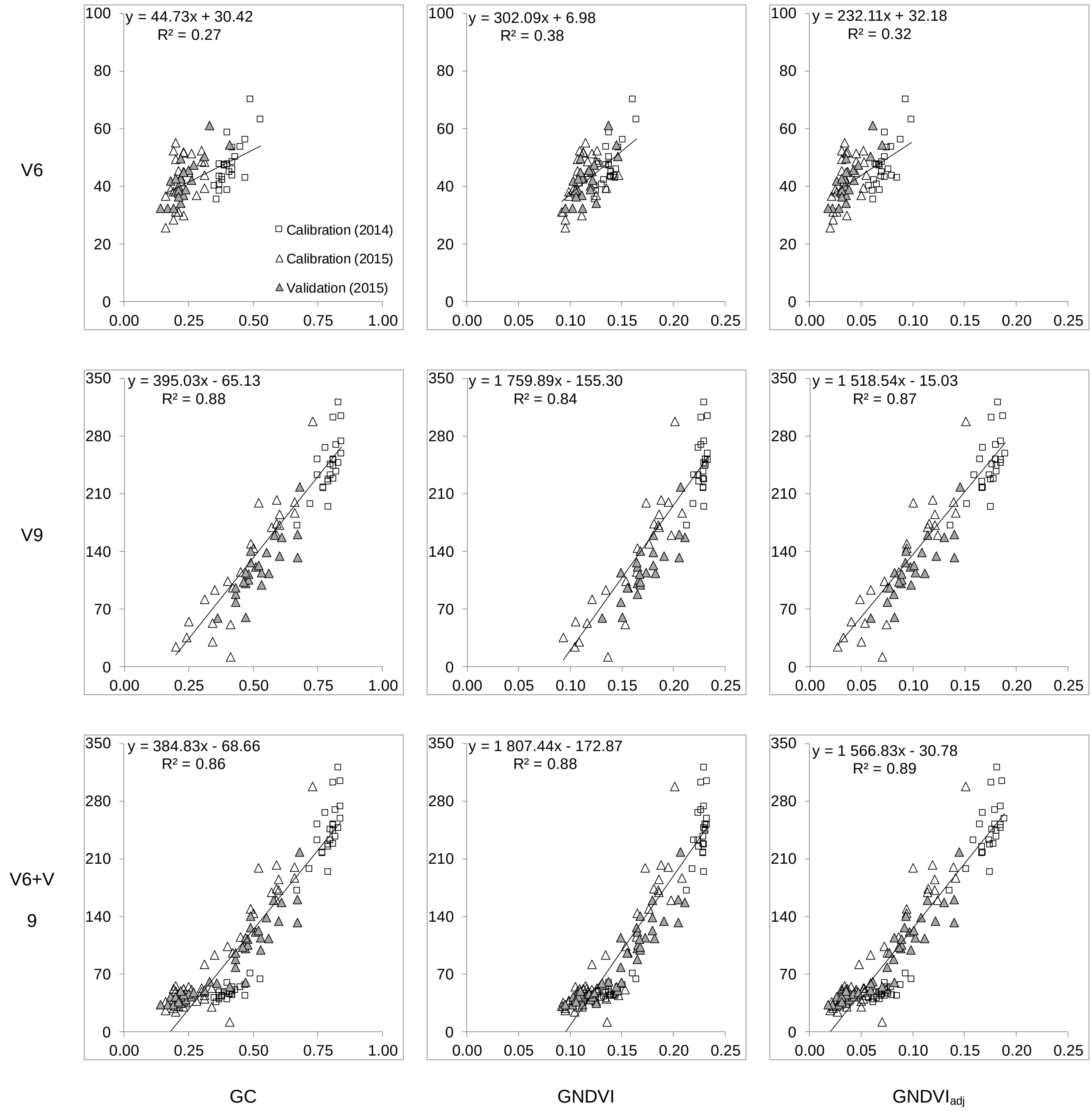

Figure 3. – Datasets used for the estimation of AGB from GC, GNDVI and $GNDVI_{adj}$.

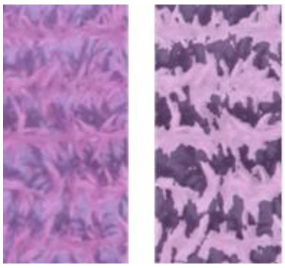

Figure 4. – the original image showing maize leaves, soil and shadowed soil (on the left) and the vegetation mask applied to calculate GC (on the right). The darker part of the mask identifies soil and shadows pixels, eliminated by the segmentation process.

Table 1. Measured and estimated maize variables as a result of fertilization. Letters indicate significant differences among treatments within year, phenological stage and variable ($P < 0.05$) (HSD Tukey test).

Year	DVS[a]	Variable[b]	Units	Treatment									
				CON	AS	DSMM	LF	SF	US	AS_{35}	AS_{70}	AS_{150}	CAN_{150}
2014	V6	AGB	g DM m^{-2}	42a	42a	45a	49ab	58b	49ab	n.a. [c]	n.a.	n.a.	n.a.
		Nc	g N 100 g DM^{-1}	3.1a	3.5a	3.7a	3.7a	3.4a	3.4a	n.a.	n.a.	n.a.	n.a.
		Nu	g N m^{-2}	1.3a	1.5ab	1.7ab	1.8ab	2.0b	1.7ab	n.a.	n.a.	n.a.	n.a.
		BNDVI	–	0.12a	0.12ab	0.12ab	0.12ab	0.13b	0.12ab	n.a.	n.a.	n.a.	n.a.
		GNDVI	–	0.13a	0.13a	0.14a	0.14a	0.16b	0.14a	n.a.	n.a.	n.a.	n.a.
		GC	–	0.37a	0.38a	0.40a	0.41a	0.49b	0.41a	n.a.	n.a.	n.a.	n.a.
		$BNDVI_{adj}$	–	0.06a	0.06ab	0.06ab	0.07b	0.08c	0.07ab	n.a.	n.a.	n.a.	n.a.
		$GNDVI_{adj}$	–	0.06a	0.06ab	0.07ab	0.07b	0.09c	0.07ab	n.a.	n.a.	n.a.	n.a.
	V9	AGB	g DM m^{-2}	212a	242a	244a	248a	277a	240a	n.a.	n.a.	n.a.	n.a.
		Nc	g N 100 g DM^{-1}	2.0a	2.7b	2.5ab	2.5ab	2.3ab	2.4ab	n.a.	n.a.	n.a.	n.a.
		Nu	g N m^{-2}	4.3a	6.4a	6.2a	6.3a	6.3a	5.7a	n.a.	n.a.	n.a.	n.a.
		BNDVI	–	0.16a	0.15a	0.16a	0.16a	0.16a	0.16a	n.a.	n.a.	n.a.	n.a.
		GNDVI	–	0.22a	0.23b	0.23b	0.23b	0.23b	0.23b	n.a.	n.a.	n.a.	n.a.
		GC	–	0.74a	0.80a	0.81a	0.80a	0.82a	0.79a	n.a.	n.a.	n.a.	n.a.
		$BNDVI_{adj}$	–	0.13a	0.13ab	0.13ab	0.13ab	0.14b	0.13ab	n.a.	n.a.	n.a.	n.a.
		$GNDVI_{adj}$	–	0.16a	0.17a	0.18a	0.18a	0.18a	0.18a	n.a.	n.a.	n.a.	n.a.
2015	V6	AGB	g DM m^{-2}	35a	42ab	41ab	40ab	53b	41ab	46ab	48ab	43b	48b
		Nc	g N 100 g DM^{-1}	3.3a	3.3a	3.5ab	3.5abc	3.6abcd	3.4a	3.9abcd	3.9cd	3.6d	3.8bcd
		Nu	g N m^{-2}	1.2a	1.4ab	1.4ab	1.4ab	1.9b	1.4ab	1.8ab	1.9b	1.6b	1.8b
		BNDVI	–	0.11a	0.12a	0.12a	0.12ab	0.14b	0.12ab	0.13ab	0.12ab	0.12ab	0.12ab
		GNDVI	–	0.10a	0.11a	0.11a	0.12a	0.14b	0.11a	0.12a	0.11ab	0.12a	0.12a
		GC	–	0.19a	0.21a	0.21a	0.24a	0.32b	0.22a	0.26a	0.24a	0.23a	0.25a
		$BNDVI_{adj}$	–	0.03a	0.03a	0.03a	0.04a	0.05b	0.04a	0.04a	0.04ab	0.04a	0.04a
		$GNDVI_{adj}$	–	0.03a	0.03a	0.03a	0.04a	0.06b	0.04a	0.04a	0.04a	0.04a	0.04a
	V9	AGB	g DM m^{-2}	86a	102ab	116ab	112ab	168bcd	128abc	204abc	186d	132cd	127abc
		Nc	g N 100 g DM^{-1}	2.4a	2.3a	2.5ab	2.4a	2.5ab	2.5ab	3.0ab	3.3bc	2.5c	2.8abc
		Nu	g N m^{-2}	2.0a	2.4a	2.8a	2.7a	4.2ab	3.1a	6.1a	6.2b	3.4b	3.6a
		BNDVI	–	0.12a	0.13ab	0.14ab	0.13ab	0.15b	0.13ab	0.14ab	0.14ab	0.13ab	0.12a
		GNDVI	–	0.15a	0.16ab	0.18abc	0.17abc	0.20c	0.17abc	0.19abc	0.19bc	0.17bc	0.16bc
		GC	–	0.43a	0.46ab	0.57abc	0.53abc	0.63c	0.50abc	0.62abc	0.59c	0.49bc	0.48abc
		$BNDVI_{adj}$	–	0.06a	0.07ab	0.09abc	0.08abc	0.10c	0.08abc	0.10abc	0.09bc	0.08bc	0.07ab
		$GNDVI_{adj}$	–	0.08a	0.08ab	0.11abc	0.10abc	0.13c	0.10abc	0.13abc	0.12c	0.09bc	0.09abc

[a]Maize developments stage according to Ritchie et al. (1993).
[b]AGB, above ground biomass; Nc, plant N concentration; Nu, plant N uptake; BNDVI, Blue Normalized Difference Vegetation Index; GNDVI, Green Normalized Difference Vegetation Index; GC, ground cover; $BNDVI_{adj}$, adjusted Blue Normalized Difference Vegetation Index; $GNDVI_{adj}$, adjusted Green Normalized Difference Vegetation Index.

[c]not available in 2014 because it was a treatment added in 2015.

Table 2. Statistics of calibration and validation datasets used to estimate maize variables.

DVS[a]	Model	Statistic	Variable[b]							
			AGB (g DM m^{-2})	Nc (g 100 g DM^{-1})	Nu (g N m^{-2})	BNDVI –	GNDVI –	GC –	$BNDVI_{adj}$ –	$GNDVI_{adj}$ –
V6	Calibration	Range	26-70	2.8-4.1	0.9-2.6	0.10-0.15	0.09-0.16	0.16-0.53	0.02-0.08	0.02-0.10
		Mean±sd[c]	45±9	3.6±0.3	1.6±0.4	0.12±0.01	0.13±0.02	0.32±0.10	0.05±0.02	0.05±0.02
		Median	45	3.6	1.6	0.12	0.13	0.33	0.05	0.06
		n	48	48	48	48	48	48	48	48
	Validation	Range	32-61	3.1-3.6	1.0-2.2	0.11-0.14	0.10-0.15	0.14-0.41	0.02-0.07	0.02-0.07
		Mean±sd	42±7	3.4±0.1	1.4±0.3	0.12±0.01	0.12±0.01	0.23±0.06	0.04±0.01	0.04±0.01
		Median	42	3.4	1.4	0.12	0.11	0.22	0.03	0.03
		n	24	24	24	24	24	24	24	24
V9	Calibration	Range	18-320	1.7-3. 5	0.4-9.4	0.09-0.16	0.09-0.23	0.20-0.84	0.02-0.14	0.03-0.19
		Mean±sd	184±83	2.6±0.4	4.8±2.2	0.14±0.02	0.19±0.04	0.63±0.20	0.10±0.04	0.13±0.05
		Median	199	2.6	5.2	0.15	0.21	0.70	0.12	0.15
		n	48	48	48	48	48	48	48	48
	Validation	Range	59-218	2.0-2.9	1.5-5.3	0.11-0.15	0.13-0.21	0.36-0.68	0.05-0.11	0.06-0.15
		Mean±sd	119±35	2.4±0.2	2.9±0.8	0.13±0.01	0.17±0.02	0.52±0.08	0.08±0.02	0.10±0.02
		Median	114	2.4	2.8	0.13	0.17	0.50	0.08	0.10
		n	24	24	24	24	24	24	24	24
V6+V9	Calibration	Range	12-320	1.7-4.1	0.4-9.4	0.09-0.16	0.09-0.23	0.16-0.84	0.02-0.14	0.02-0.19
		Mean±sd	114±91	3.1±0.6	3.2±2.2	0.13±0.02	0.16±0.05	0.48±0.22	0.08±0.04	0.09±0.05
		Median	53	3.2	2.0	0.12	0.14	0.42	0.06	0.07
		n	96	96	96	96	96	96	96	96
	Validation	Range	32-218	2.0-3.6	1.0-5.3	0.11-0.15	0.10-0.21	0.14-0.68	0.02-0.11	0.02-0.15
		Mean±sd	80±46	2.9±0.5	2.2±1.0	0.13±0.01	0.14±0.03	0.38±0.16	0.06±0.03	0.07±0.04
		Median	59	3.0	1.8	0.13	0.15	0.39	0.06	0.07
		n	48	48	48	48	48	48	48	48

[a]Maize developments stage according to Ritchie et al., (1993).
[b]AGB, above ground biomass; Nc, plant N concentration; Nu, plant N uptake; GC, ground cover; GNDVI, Green Normalized Difference Vegetation Index; $GNDVI_{adj}$, adjusted Green Normalized Difference Vegetation Index; BNDVI, Blue Normalized Difference Vegetation Index; $BNDVI_{adj}$, adjusted Blue Normalized Difference Vegetation Index.
[c]sd, standard deviation.

Table 3. – Performances of regression models used to estimate maize variables applied to the calibration and validations data sets. Reported statistics are the coefficient of determination (R^2) and the Relative Root Mean Square Error (RRMSE). Significance of linear regressions is reported closed to calibration R^2 as follow: not significant (ns), $P < 0.05$ (*), $P < 0.01$ (**).

Dependent variable[a]	DVS[b]	Statistic	Dataset														
			Calibration							Validation							
			Independent variable[c]														
			BNDVI	GNDVI	GC	$BNDVI_{adj}$	$GNDVI_{adj}$	CLGRM	$CLGRM_{veg}$	BNDVI	GNDVI	GC	$BNDVI_{adj}$	$GNDVI_{adj}$	CLGRM	$CLGRM_{veg}$
AGB	V6	R^2	0.25**	0.38**	0.27**	0.30**	0.32**	0.94	0.8	0.34	0.49	0.64	0.67	0.69	0.46	0.15
		RRMSE	17	16	17	17	17	5	9	16	12	13	12	12	15	18
	V9	R^2	0.80**	0.84**	0.88**	0.86**	0.87**	0.89	0.94	0.61	0.67	0.68	0.71	0.71	0.58	0.46
		RRMSE	20	18	16	17	16	15	11	41	31	24	24	22	33	49
	V6+V9	R^2	0.73**	0.88**	0.86**	0.85**	0.89**	0.95	0.99	0.49	0.87	0.88	0.88	0.9	0.87	0.85
		RRMSE	42	28	30	31	27	18	9	54	31	31	26	25	40	41
Nu	V6	R^2	0.19**	0.21**	0.11*	0.14**	0.15**	0.9	0.76	0.33	0.5	0.59	0.64	0.67	0.41	0.05
		RRMSE	21	21	22	22	22	7	11	21	15	16	15	15	26	28
	V9	R^2	0.59**	0.66**	0.69**	0.64**	0.68**	0.8	0.84	0.54	0.6	0.63	0.64	0.65	0.5	0.39
		RRMSE	30	28	26	28	26	20	18	52	42	35	35	32	64	76
	V6+V9	R^2	0.64**	0.78**	0.77**	0.74**	0.79**	0.95	0.77	0.53	0.81	0.8	0.82	0.83	0.75	0.7
		RRMSE	42	33	34	36	33	15	13	51	37	34	28	28	66	66
Nc	V6	R^2	0.01ns	0.01ns	0.06ns	0.04ns	0.03ns	0.81	0.28	0.11	0.2	0.13	0.16	0.19	0.003	0.19
		RRMSE	9	9	8	8	8	4	7	6	6	8	7	7	11	9
	V9	R^2	0.14**	0.10ns	0.08ns	0.12ns	0.08ns	0.42	0.74	0.01	0.02	0.01	0.01	0.01	0.003	0
		RRMSE	14	14	15	14	15	11	8	13	14	14	14	14	21	7
	V6+V9	R^2	0.29**	0.47**	0.47**	0.45**	0.46**	0.83	0.58	0.18	0.65	0.71	0.65	0.67	0.78	0.63
		RRMSE	17	14	14	15	15	8	13	18	16	16	17	17	16	17

[a]AGB, Above Ground Biomass; Nu, plant N uptake; Nc, N concentration.
[b]Maize development stage according to Ritchie et al., (1992).
[c]BNDVI, Blue Normalized Difference Vegetation Index; GNDVI, Green Normalized Difference Vegetation Index; GC, Ground Cover; $BNDVI_{adj}$, adjusted Blue Normalized Difference Vegetation Index; $GNDVI_{adj}$, adjusted Green Normalized Difference Vegetation Index; CLGRM, cologram; $CLGRM_{veg}$, cologram of the vegetation.